Study of Ga-Polar and N-Polar GaN-Based Green VCSELs by Simulation

Ya-Chao Wang [ORCID], Yan-Hui Chen, Zhong-Ming Zheng [ORCID], Tao Yang, Yang Mei [ORCID], Lei-Ying Ying, and Bao-Ping Zhang [ORCID]

Abstract—**Gallium Nitride (GaN)-based vertical-cavity surface-emitting lasers (VCSELs) in green spectral region face the difficulty of the "green gap". One of the main obstacles is the strong polarization electric field in GaN-based materials, which leads to a strong quantum confinement Stark effect (QCSE) and reduces the efficiency of radiative recombination. In this study, we systemically simulated and compared the optical and electrical performance of GaN-based green VCSELs based on Ga-polar and N-polar InGaN quantum wells (QWs) by using the software of PICS3D. The results show that the light-output power of N-polar VCSEL is greatly improved by 183% compared to Ga-polar VCSEL at an injection current of 20 mA, while the threshold current is reduced by 49%. The improved performance is mainly attributed to: 1) the decreased QCSE; 2) the more efficient carrier injection, and 3) the reduced carrier leakage in N-polar devices. The results of this study suggest that N-polar based GaN is promising for the realization of high-performance green VCSELs, which can provide a guidance for the fabrication of high-power green VCSELs.**

Index Terms—**VCSEL, gallium nitride, N-polar, simulation.**

I. INTRODUCTION

GAN-BASED VCSELs are attracting significant attention due to their compact size, low threshold current, ability to produce single longitudinal mode output, and their suitability for implementation in two-dimensional array packages. These characteristics make them highly promising for various applications, including solid state lighting, displays, data communications, and high-density optical storage [1], [2], [3], [4]. The world's first electrically injected GaN-based VCSEL was achieved in 2008 [5], and research on GaN-based VCSELs has made significant progress in past decades. However, most studies mainly focus on the blue-violet wavelengths, and for the green band with important practical value, GaN-based VCSELs are developing slowly. Only a few institutions have achieved GaN-based green

VCSELs, but with much lower output power than their blue and violet counterparts [6], [7], [8], [9]. InGaN QWs grown along the c-axis [0001] direction are commonly used as the active region in GaN-based VCSELs. For devices emitting in green, more Indium needs to be incorporated into the active region, resulting a larger lattice mismatch between InGaN and GaN, and higher density of defects and dislocations. In addition, due to the strong spontaneous polarization and the piezoelectric polarization caused by lattice mismatch between InN and GaN, the total polarization electric field in the green InGaN QWs can be as high as 5–10 MV/cm [10]. Such a large polarization electric field will cause strong QCSE [11]. The large QCSE not only leads to the separation of the electron-hole wave functions, but also reduces the quantum barrier height, which weakens the confinement of the carriers, and makes them to escape from the QWs more easily. As a result, the luminescence efficiency is drastically reduced in the green wavelength region, which is known as "green gap" [12].

Using semi-polar or non-polar GaN substrates for green light VCSEL fabrication is also a good choice [13]. Considering the production cost, however, growth on c-plane is preferred. According to the different arrangement of Ga and N atoms along the c-axis in GaN, it can be divided into Ga-polar along the [0001] direction and N-polar along the [000$\bar{1}$] direction [14]. Hence N-polar and Ga-polar GaN materials have internally opposite polarization directions and different properties. In 2011, Akyol et al. [15]. fabricated a N-polar GaN-based green light emitting diode (LED) by plasma-assisted molecular beam epitaxy (PAMBE). They observed that the N-polar structure effectively reduced the width of the depletion layer, leading to a lower turn-on voltage. In 2015, Feng et al. [16]. demonstrated N-polar and Ga-polar GaN-based LEDs using metal-organic chemical vapor deposition (MOCVD) respectively. They revealed that the N-polar LED exhibited more efficient carrier relaxation and faster carrier recombination. In 2022 Li et al. [17]. Numerically investigated the performance of Ga-polar and N-polar green LEDs by using APYSYS software. They found that N-polar LED shows a significant increase in output power and internal quantum efficiency. Importantly, N-polarity has also been identified as favoring the growth of high In-composition InGaN films [18], [19], [20].

It has also been reported that the point defect density at the interface of N-polar QW structures is higher than Ga-polar structures [21]. However, with the development of high-quality
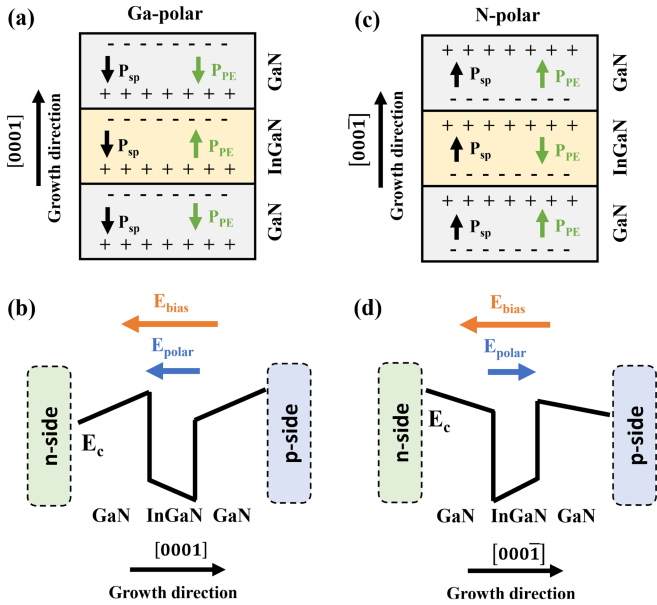
Fig. 1. (a) P_{SP} and P_{PE} of GaN and InGaN in Ga-polar; (b) applied electric field and energy band tilt in Ga-polar; (c) P_{SP} and P_{PE} of GaN and InGaN in N-polar; (d) applied electric field and energy band tilt in N-polar.
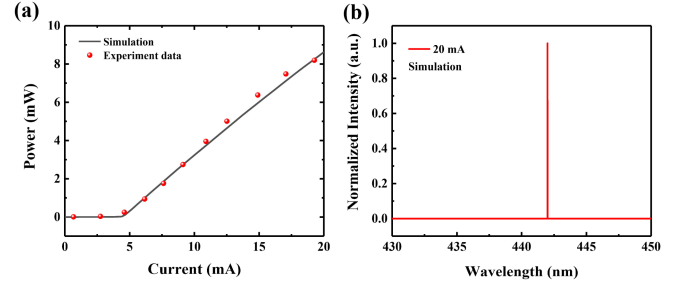

Fig. 2. (a) P-I curves for experiment (Ref. [22]) and simulation; (b) simulated emission spectrum under 20 mA CW operation.

TABLE I
KEY MATERIAL PARAMETERS OBSERVED IN EXPERIMENT AND
USED IN SIMULATION

	Material	Experiment	Simulation
n-DBR	AlInN/GaN	42 pairs	42 pairs
n-GaN	n-GaN	660 nm	680 nm
MQW	InGaN/GaN	39 nm	39 nm
EBL	p-AlGaN	20 nm	20 nm
p-GaN	p-GaN	-	84 nm
SiO$_2$	SiO$_2$	20 nm	20 nm
ITO	ITO	20 nm	20 nm
p-DBR	SiO$_2$/Nb$_2$O$_5$	10.5 pairs	10.5pairs

N-polar GaN epitaxy, it may be beneficial for N-polar GaN to enhance the performance of long-wavelength GaN-based VCSELs. Therefore, it is necessary to investigate and compare the optoelectronic properties of Ga-polar and N-polar GaN-based green VCSELs.

In this study, the simulation and analysis of the optical and electrical properties of Ga-polar and N-polar GaN-based VC-SELs in the green wavelength range were conducted by the commercial software of Crosslight PICS3D. The results show that N-polar GaN-based VCSELs can effectively increase the efficiency of carrier injection into the active region, meanwhile, reduce the carrier leakage compared to Ga-polar VCSEL. The weakened QCSE and improved overlap of carrier wave functions result in a higher radiation recombination rate of the InGaN QWs. With all these improvements, the light-output power of N-polar VCSEL is increased by 183% compared to Ga-polar VCSEL, while the threshold current is reduced by 49%. The advantages of N-polar GaN in green VCSELs are theoretically illustrated, providing a guidance for the future development of high-power green VCSELs.

II. DEVICE STRUCTURE AND SIMULATION PARAMETERS

There is a spontaneous polarization (P_{SP}) along the c-axis in wurtzite GaN, and the P_{SP} is in the direction of [000$\bar{1}$]. For InGaN/GaN QWs, there is also a piezoelectric polarization (P_{PE}) with them, and the direction is opposite in well and barrier layers because of the different type of strain, as shown in Fig. 1(a) and (c). The total polarized electric field is determined by the combination of P_{SP} and the P_{PE}, and the direction is [0001] in the GaN layers, and [000$\bar{1}$] in the InGaN layers with high Indium content. During device operation, the applied bias electric field (E_{bias}) points from p-GaN to n-GaN, so that it is coincides

with the polarized electric field (E_{polar}) in the InGaN QWs in Ga-polar VCSEL, as shown in Fig. 1(b). The tilt of the energy band in the QWs is intensified due to the superimposed effect of the two electric fields, decreasing the overlap of the electron-hole wave functions. In contrast, the E_{polar} is opposite to the E_{bias} in N-polar device, as shown in Fig. 1(d). The forward bias assists the band diagram in QWs to approach flat-band condition, reducing the QCSE and favors the radiative recombination of electron-hole pairs [15].

To verify the accuracy of our model, we first simulate a reference device report by Kuramoto et al. [22]. Crosslight PICS3D was used to simulate the optical and electrical properties of VC-SELs, which contains drift-diffusion equations, Schrödinger and Poisson's equations, etc. The Auger recombination coefficient was set to be 1.4×10^{-31} cm^{6}s^{-1} to account for Auger recombination in the material, and the Shockley-Read-Hall (SRH) lifetime is 1×10^{-8} s [23], [24]. The polarization level was set as 40% to approximate the polarized charge at the interface [25]. The offset ratio of conduction/valence band in the MQWs was set to be 70:30. To account for optical losses, the average optical background loss of the n-GaN, MQWs, EBL, and p-GaN layers in the cavity was set to 1000 m^{-1} [26]. Fig. 2(a) shows the power-current (P-I) characterization of experimental VCSEL (red dot) and simulated VCSEL (black line). The results of the experiment and the simulation are in good agreement. The emission wavelength of the VCSEL is 442 nm, as shows in Fig. 2(b). The emitting aperture is 8 μm and the cavity length is 5 λ. Table I lists the key material parameters used in both the experiment and simulation.

In our proposed device structure, as shown in Fig. 3, we incorporate a dual dielectric Distributed Bragg Reflector (DBR) structure. The bottom DBR consists of 12.5 periods of SiO$_2$/TiO$_2$,
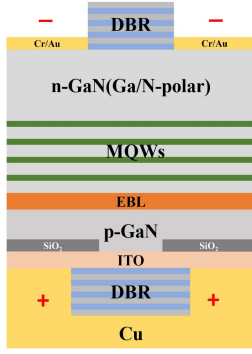
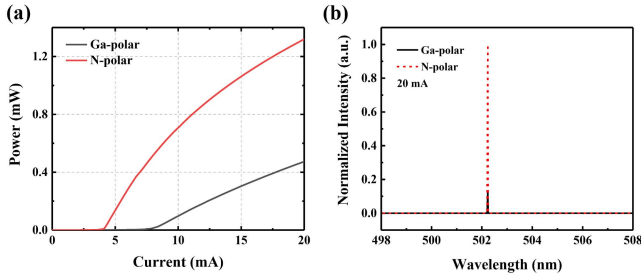Fig. 3. Ga-polar or N-polar GaN-based VCSELs device structure.

Fig. 4. (a) P-I curves and (b) emission spectrum for Ga-polar VCSEL and N-polar VCSEL.
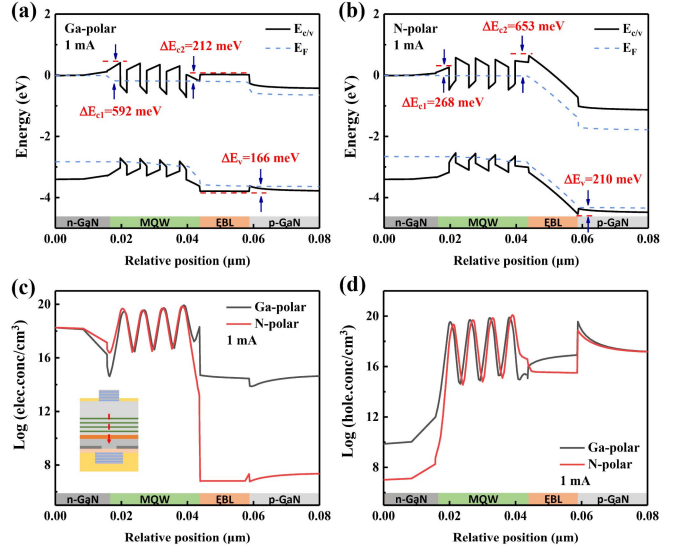

Fig. 5. (a) Energy band diagram at 1 mA in Ga-polar VCSEL, the dashed line is the quasi-Fermi level; (b) energy band diagram at 1 mA in N-polar VCSEL; (c) electron concentration distribution in logarithmic coordinates; (d) hole concentration distribution in logarithmic coordinates.

while the top DBR consists of 6 periods of SiO_2/TiO_2. To facilitate current spreading, we utilize a 20 nm-thick Indium Tin Oxide (ITO) layer as the current spreading layer. Additionally, a 10 nm-thick layer of SiO_2 is employed as the current confinement layer. The device features an optical emission aperture, also serving as the current confinement aperture, with a diameter of 5 μm. The emission wavelength of the device is targeted at 502.2 nm. It is worth noting that the only difference between the Ga-polar and N-polar GaN-based VCSELs is the crystal orientation. The detailed parameters of the epi-layers and material used in the device can be found in our previous work [27].

III. RESULTS AND DISCUSSION

Fig. 4(a) shows the P-I curves for the Ga-polar and N-polar VCSEL. The luminescence performance of the N-polar VCSEL is significantly improved. The output power of the N-polar VCSEL is 1.30 mW at 20 mA, which is 183% higher than the 0.46 mW of the Ga-polar VCSEL. In addition, the threshold current of the N-polar VCSEL is 4.1 mA, which is also much lower than the 8.0 mA of the Ga-polar VCSEL (decreased by ∼49%). The emission wavelength of the Ga-polar and N-polar VCSEL is 502.2 nm, as shows in Fig. 4(b).

To illustrate the reason for the improved luminescence performance in N-polar VCSEL, the energy band of two structures was analyzed. Fig. 5(a) and (b) show the energy band diagrams of Ga-polar VCSEL and N-polar VCSEL at 1 mA (below threshold), respectively. The barrier for electron injection (ΔE_{c1}) in Ga-polar VCSEL is 592 meV, while ΔE_{c1} is only 267 meV in N-polar VCSEL, reducing by 55%. The smaller ΔE_{c1} is

beneficial for the electron injection into the MQWs. At the same time, the effective barrier height for EBL in the conduction band (ΔE_{c2}) is 212 meV in Ga-polar VCSEL. But this value is 653 meV in N-polar VCSEL, which is improved by 208%. The increased ΔE_{c2} helps to suppress electron leakage from active region into the p-GaN. The difference between ΔE_{c1} and ΔE_{c2} in the two VCSELs can be attributed to the opposite direction of the energy band tilt in the InGaN layers. In N-polar VCSEL, the conduction band of InGaN QW layers tilt upwarping from left to right side. The electrons preferentially fill the lower energy level of the conduction band, and this will induce a smaller barrier potential for the GaN barrier layer on left side and a larger barrier potential on right side. Therefore, the injection of electrons and the suppression of their leakage to p-GaN can be both improved in N-polar VCSEL. The injection efficiency of holes can also be improved in N-polar VCSEL. Due to the direction of E_{polar} in the EBL is the same as E_{bias}, the valence band of EBL is tilted upwarping towards the MQWs, and the energy of the holes is gradually decreased from p-GaN to the MQWs. Therefore, the holes injected in N-polar VCSEL is only hindered by a very thin barrier at the EBL/p-GaN interface. They can easily reach the MQWs by tunneling effect at the EBL/p-GaN interface and then drift accelerately in the EBL with the tilted valance band. So, in N-polar VCSEL, the hole concentration at the EBL/p-GaN interface is less than Ga-polar VCSEL, which leads to an increase in the difference between the valence band and the Fermi energy level, i.e., ΔE_v. The values of ΔE_{c1}, ΔE_{c2} and ΔE_v of the two VCSELs are shown in Table II. In addition, the effective barrier potential for electrons from n-side towards p-side and holes from p-side towards n-side in each QWs for Ga-polar and N-polar VCSEL are presented in Tables III and IV (QWs are numbered in order from the n-side to the p-side). It can be seen that N-polar VCSEL has an increased barrier height in each QWs for both electrons and holes compared to

TABLE II
SIMULATED POTENTIAL BARRIER OF ELECTRONS AND HOLES FOR GA-POLAR AND N-POLAR VCSEL

Sample	ΔE_{c1}	ΔE_{c2}	ΔE_v
Ga-polar VCSEL	592 meV	212 meV	166 meV
N-poalr VCSEL	268 meV	653 meV	210 meV

TABLE III
EFFECTIVE POTENTIAL BARRIER HEIGHT FOR ELECTRONS IN MQWS

Sample	First QW	Second QW	Third QW	Fourth QW
Ga-polar VCSEL	574 meV	534 meV	490 meV	204 meV
N-poalr VCSEL	587 meV	573 meV	530 meV	490 meV

TABLE IV
EFFECTIVE POTENTIAL BARRIER HEIGHT FOR HOLES IN MQWS

| Sample	First QW	Second QW	Third QW	Fourth QW
Ga-polar VCSEL	459 meV	401 meV	370 meV	348 meV
N-poalr VCSEL	681 meV	413 meV	386 meV	357 meV

Fig. 6. (a) Electron concentration distribution in MQWs; (b) hole concentration distribution in MQWs; (c) electron-hole wave functions in Ga-polar QWs; (d) electron-hole wave functions in N-polar QWs; (e) radiative recombination rate at 1 mA.

Ga-polar VCSEL, which consist with the above analysis. This suggests that the active region of N-polar VCSEL has a stronger carrier localization effect than Ga-polar VCSEL, which benefits the radiative recombination and suppression of carrier leakage. Fig. 5(c) shows the electron concentration in different layers plotted in logarithmic coordinates at 1 mA. Due to the improved barrier height (ΔE_{c2}), the electron concentration of p-GaN in N-polar VCSEL decreases from 10^{14} cm^{-3} to 10^7 cm^{-3} compared to Ga-polar VCSEL. The electrons leakage to p-GaN is reduced by 7 orders of magnitude. Fig. 5(d) shows the hole concentration in logarithmic coordinates at 1 mA. The hole concentration of n-GaN in N-polar VCSEL decreases from 10^{10} cm^{-3} to 10^7 cm^{-3} compared to Ga-polar VCSEL, benefiting from the stronger carrier localization in the N-polar VCSEL. It is also worth to note that the hole concentration of EBL in the N-polar VCSEL is lower than that in Ga-polar VCSEL. It means that the holes blocked by EBL is much smaller because of the tilted valance band, and holes can be injected into the MQWs more efficient.

Fig. 6(a) and (b) show the electron and hole concentration in the MQWs at 1 mA, respectively. Compared to Ga-polar VCSEL, the N-polar VCSEL features a higher electron concentration in the first QW and a higher hole concentration in the fourth QW. This indicates that more carrier reached to the MQWs at the same injection conditions, which means the more efficient carrier injection in the N-polar VCSEL. The electrons-holes wave functions in the fourth QW of Ga-polar and N-polar VCSEL are shown in Fig. 6(c) and (d). The overlap of the wave functions (area of yellow section divided by the total area of curve integral) in N-polar VCSEL is 49.3%, which is higher than the 40.2% in the Ga-polar VCSEL (improved by ∼22.6%). The
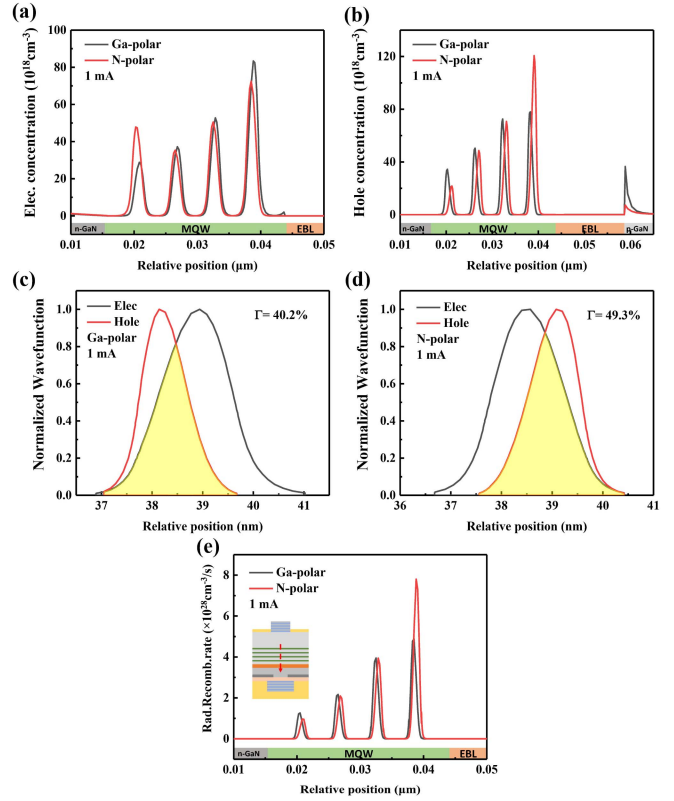
larger overlap of wave functions means a higher probability of radiative recombination. Together with the more efficient carrier injection, the radiative recombination rate is higher in N-polar VCSEL, as shown in Fig. 6(e).

The above effect is even more pronounced at high current levels. Fig. 7(a) and (b) show the electron and hole concentration in the MQWs at 20 mA, respectively. Due to the higher ΔE_{c2} in N-polar VCSEL, much more electrons are confined in the MQW, especially in the fourth QW. Fig. 7(c) and (d) show the wave function distribution in the fourth QW in the Ga-polar VCSEL and N-polar VCSEL at 20 mA (above threshold), respectively. The electron-hole wave function overlap in the Ga-polar VCSEL is 50.5%, and 66.2% in the N-polar VCSEL. Wave function overlap is improved by ∼31.1% in N-polar VCSEL at 20 mA, which is higher than the improvement of 22.6% at 1 mA. This can be explained by the fact that the direction of the polarization electric field of the MQWs in the N-polar VCSEL is opposite to the applied bias electric field. Therefore, the QCSE decreases as the applied bias electric field increases [21]. Note that the overlap of electron and hole wave function is also improved a little for the Ga-polar VCSEL under a higher bias voltage despite of the same direction of polarization induced and applied bias electric field, and this can be explained by the enhanced carrier screening effect under high current. The stimulated radiative recombination rate at 20 mA is shown in Fig. 7(e). Compared with the Ga-polar VCSEL, N-polar VCSEL exhibit a much higher
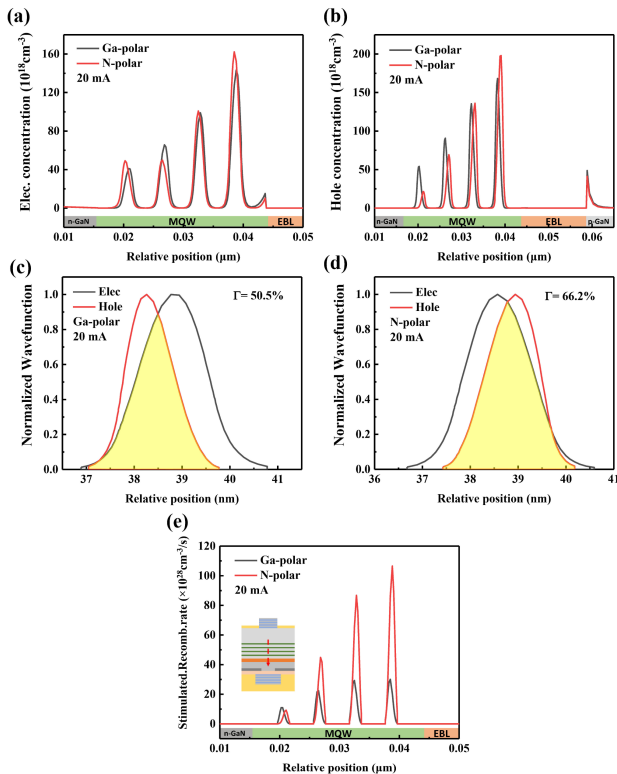
Fig. 7. (a) Electron concentration distribution in MQWs; (b) hole concentration distribution in MQWs; (c) electron-hole wave functions in fourth QW of Ga-polar VCSEL; (d) electron-hole wave functions in fourth QW of N-polar VCSEL; (e) stimulated radiative recombination rate at 20 mA.
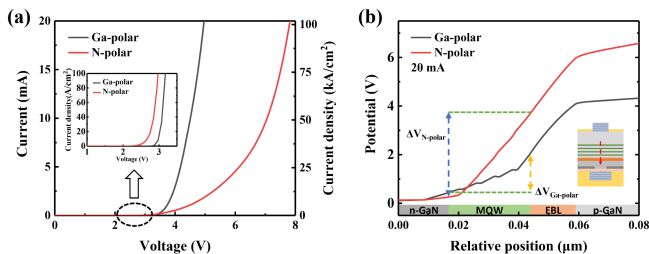

Fig. 8. (a) I-V curves for Ga-polar VCSEL and N-polar VCSEL, inset shows I-V curves at small current; (b) vertical potential distribution along the marked position for the inset schematic VCSEL.

stimulated radiative recombination rate, especially in the QWs near the p-side. This can be attributed to the more efficient carrier injection, smaller QCSE, better carrier localization and smaller carrier leakage in the active region of the N-polar VCSEL.

Fig. 8(a) shows the relationship between the injection current-voltage (I-V) curve of the Ga-polar and N-polar VCSEL. The inset shows the IV curve under small current. Due to the reduced carrier injection barrier, N-polar VCSEL have a lower turn-on voltage compared to Ga-polar VCSEL (inset of Fig. 8(a)), which is consistent with previous reports [28], [29], [30]. The voltage increase in the N-polar VCSEL are more significant than Ga-polar VCSEL under high current. To understand this behavior, the distribution the consumption of the applied voltage in the n-GaN, MQWs, EBL, and p-GaN layers at 20 mA is

plot in Fig. 8(b). Indeed, the observed larger voltage drop in the MQWs of the N-polar VCSEL compared to the Ga-polar VCSEL indicates a higher resistance in this region. This resistance can be attributed to the strong carrier localization in the MQWs of the N-polar VCSEL, especially under high injection levels [16]. The I-V properties are expected to be improved by In composition graded Quantum barrier (QB) [31], staggered QW [32] stepped EBL [33] and et.al.

IV. CONCLUSION

In summary, the optical and electrical properties of Ga-polar and N-polar GaN-based green VCSELs have been simulated and analyzed in this work. Among them, the optical output power of N-polar VCSEL is significantly improved by 183% compared to Ga-polar VCSEL at an injection current of 20 mA, while the threshold current is reduced by 49%. This optimization is due to the fact that under N-polar, the carrier injection barrier in the active region is lowered while the blocking barrier is increased, which increases the number of carriers confined in the MQWs. On the other hand, under N-polar, the polarization electric field in the InGaN QWs is in the opposite direction to the applied bias electric field, which reduces the degree of energy band tilting by superposition and increases the overlap of the wave functions, thus increasing the emission efficiency of the device. This paper provides an in-depth analysis of the mechanism behind the enhancement of optoelectronic properties by N-polar. Providing a guide for the subsequent fabrication of high-performance green VCSELs.

REFERENCES

[1] H. Yu et al., "Progress and prospects of GaN-based VCSEL from near UV to green emission," *Prog. Quantum Electron.*, vol. 57, pp. 1–19, 2018, doi: 10.1016/j.pquantelec.2018.02.001.

[2] Å. Haglund et al., "Progress and challenges in electrically pumped GaN-based VCSELs," *Proc. SPIE*, vol. 9892, pp. 161–180, 2016.

[3] R. R. Hainich and O. Bimber, *Displays: Fundamentals & Applications*. Boca Raton, FL, USA: CRC Press, 2016.

[4] A. Liu, P. Wolf, J. A. Lott, and D. Bimberg, "Vertical-cavity surface-emitting lasers for data communication and sensing," *Photon. Res.*, vol. 7, no. 2, pp. 121–136, 2019, doi: 10.1364/prj.7.000121.

[5] T.-C. Lu, C.-C. Kao, H.-C. Kuo, G.-S. Huang, and S.-C. Wang, "CW lasing of current injection blue GaN-based vertical cavity surface emitting laser," *Appl. Phys. Lett.*, vol. 92, no. 14, 2008, Art. no. 141102, doi: 10.1063/1.2908034.

[6] Y. Mei et al., "Quantum dot vertical-cavity surface-emitting lasers covering the 'green gap'," *Light: Sci. Appl.*, vol. 6, no. 1, Jan. 2017, Art. no. e16199, doi: 10.1038/lsa.2016.199.

[7] K. Terao et al., "Blue and green GaN-based vertical-cavity surface-emitting lasers with AlInN/GaN DBR," in *Proc. Gallium Nitride Mater. and Devices XVI*, 2021, Art. no. 116860E.

[8] T. Hamaguchi, "GaN-based VCSELs with a monolithic curved mirror: Challenges and prospects," *Photonics*, vol. 10, no. 4, 2023, Art. no. 470, doi: 10.3390/photonics10040470.

[9] T. Yang et al., "Green vertical-cavity surface-emitting lasers based on InGaN quantum dots and short cavity," *Nano-Micro Lett.*, vol. 15, no. 1, 2023, Art. no. 223, doi: 10.1007/s40820-023-01189-0.

[10] J. Lähnemann et al., "Direct experimental determination of the spontaneous polarization of GaN," *Phys. Rev. B*, vol. 86, no. 8, 2012, Art. no. 081302, doi: 10.1103/PhysRevB.86.081302.

[11] M. Leroux et al., "Quantum confined stark effect due to built-in internal polarization fields in (Al, Ga) N/GaN quantum wells," *Phys. Rev. B*, vol. 58, no. 20, 1998, Art. no. R13371.

[12] T. Langer et al., "Origin of the 'green gap': Increasing nonradiative recombination in indium-rich GaInN/GaN quantum well structures," *Physica Status Solidi*, vol. 8, no. 7/8, pp. 2170–2172, 2011, doi: 10.1002/pssc.201001051.

[13] T. Hamaguchi et al., "Room-temperature continuous-wave operation of green vertical-cavity surface-emitting lasers with a curved mirror fabricated on {20−21} semi-polar GaN," *Appl. Phys. Exp.*, vol. 13, no. 4, 2020, Art. no. 041002, doi: 10.35848/1882-0786/ab7bc8.

[14] O. Ambacher et al., "Two-dimensional electron gases induced by spontaneous and piezoelectric polarization charges in N-and Ga-face AlGaN/GaN heterostructures," *J. Appl. Phys.*, vol. 85, no. 6, pp. 3222–3233, 1999.

[15] F. Akyol, D. N. Nath, E. Gür, P. S. Park, and S. Rajan, "N-polar III–nitride green (540 nm) light emitting diode," *Japanese J. Appl. Phys.*, vol. 50, no. 5, 2011, Art. no. 052101, doi: 10.1143/jjap.50.052101.

[16] S.-W. Feng, P.-H. Liao, B. Leung, J. Han, F.-W. Yang, and H.-C. Wang, "Efficient carrier relaxation and fast carrier recombination of N-polar InGaN/GaN light emitting diodes," *J. Appl. Phys.*, vol. 118, no. 4, 2015, Art. no. 043104, doi: 10.1063/1.4927421.

[17] Y. Li, Y. Jiang, H. Jia, W. Wang, R. Yang, and H. Chen, "Superior optoelectronic performance of N-polar GaN LED to Ga-polar counterpart in the 'green gap' range," *IEEE Access*, vol. 10, pp. 95565–95570, 2022, doi: 10.1109/access.2022.3204668.

[18] K. Xu and A. Yoshikawa, "Effects of film polarities on InN growth by molecular-beam epitaxy," *Appl. Phys. Lett.*, vol. 83, no. 2, pp. 251–253, 2003.

[19] K. Wang, T. Araki, M. Takeuchi, E. Yoon, and Y. Nanishi, "Selective growth of N-polar InN through an in situ AlN mask on a sapphire substrate," *Appl. Phys. Lett.*, vol. 104, no. 3, 2014, Art. no. 032108, doi: 10.1063/1.4859615.

[20] N. Fichtenbaum et al., "Electrical characterization of p-type N-polar and Ga-polar GaN grown by metalorganic chemical vapor deposition," *Appl. Phys. Lett.*, vol. 91, no. 17, 2007, Art. no. 172105.

[21] S. Mohanty, K. Khan, and E. Ahmadi, "N-polar GaN: Epitaxy, properties, and device applications," *Prog. Quantum Electron.*, vol. 87, 2023, Art. no. 100450, doi: 10.1016/j.pquantelec.2022.100450.

[22] M. Kuramoto et al., "High-output-power and high-temperature operation of blue GaN-based vertical-cavity surface-emitting laser," *Appl. Phys. Exp.*, vol. 11, 2018, Art. no. 112101.

[23] S. Hang et al., "On the origin for the hole confinement into apertures for GaN-based VCSELs with buried dielectric insulators," *Opt Exp.*, vol. 28, no. 6, pp. 8668–8679, Mar. 2020, doi: 10.1364/OE.385787.

[24] P. Mackowiak and W. Nakwaski, "Designing guidelines for possible continuous-wave-operating nitride vertical-cavity surface-emitting lasers," *J. Phys. D: Appl. Phys.*, vol. 33, no. 6, 2000, Art. no. 642.

[25] X. Qiu et al., "Enhancing the lateral current injection by modulating the doping type in the P-type hole injection layer for InGaN/GaN vertical cavity surface emitting lasers," *Opt Exp.*, vol. 28, no. 12, pp. 18035–18048, Jun. 2020, doi: 10.1364/OE.396482.

[26] L. Han et al., "Impact of P-AlGaN/GaN hole injection layer on GaN-based vertical cavity surface emitting laser diodes," *Chin. Opt. Lett.*, vol. 20, no. 3, 2022, Art. no. 031402, doi: 10.3788/col202220.031402.

[27] Y. Wang, T. Yang, L. Shi, Y. Chen, Y. Mei, and B.-P. Zhang, "Simulation of performance enhancement of GaN-based VCSELs by composition gradient InGaN last-quantum barrier," *Semicond. Sci. Technol.*, vol. 38, no. 12, 2023, Art. no. 125003, doi: 10.1088/1361-6641/ad03fd.

[28] S. I. Rahman, Z. Jamal-Eddine, A. M. D. M. Xavier, R. Armitage, and S. Rajan, "III-nitride P-down green (520 nm) light emitting diodes with near-ideal voltage drop," *Appl. Phys. Lett.*, vol. 121, no. 2, 2022, Art. no. 021102, doi: 10.1063/5.0093403.

[29] G. Deng et al., "Simulation and fabrication of N-polar GaN-based blue-green light-emitting diodes with P-type AlGaN electron blocking layer," *J. Mater. Sci.: Mater. Electron.*, vol. 29, no. 11, pp. 9321–9325, 2018, doi: 10.1007/s10854-018-8962-y.

[30] M. Usman, U. Mushtaq, M. Munsif, A.-R. Anwar, and M. Kamran, "Enhancement of the optoelectronic performance of P-down multiquantum well N-GaN light-emitting diodes," *Physica Scripta*, vol. 94, no. 10, 2019, Art. no. 105808, doi: 10.1088/1402-4896/ab28c0.

[31] C. Jia, C. He, Z. Liang, and Q. Wang, "Improvement of radiative recombination rate and efficiency droop of InGaN light emitting diodes with in-component-graded InGaN barrier," *Physica Status Solidi*, vol. 218, no. 20, 2021, Art. no. 2100351, doi: 10.1002/pssa.202100351.

[32] X. Zhao, B. Tang, L. Gong, J. Bai, J. Ping, and S. Zhou, "Rational construction of staggered InGaN quantum wells for efficient yellow light-emitting diodes," *Appl. Phys. Lett.*, vol. 118, no. 18, 2021, Art. no. 182102, doi: 10.1063/5.0043240.

[33] F. Zhao et al., "Simulation and theoretical study of AlGaN-based deep-ultraviolet light-emitting diodes with a stepped electron barrier layer," *Amer. Inst. Phys. Adv.*, vol. 12, 2022, Art. no. 125003, doi: 10.1063/5.0127070.